JPEDAV (2005) 26:458-465
DOI: 10-1361/154770305X66538
1547-7037/$19.00 ©ASM International

Self-Diffusion in Nanoscale Structures Measured by Neutron Reflectometry

Mukul Gupta, Ajay Gupta, Rachana Gupta, and Thomas Gutberlet

(Submitted July 12, 2005)

Neutron reflectometry (NR) is an attractive tool for probing self-diffusion on a nanometer-length scale. The depth resolution available with NR is in the subnanometer range, which is due to contrast among the isotopes of an element, and NR provides a unique opportunity to probe self-diffusion in nanometer-range structures. Self-diffusion measurements in FeZr amorphous and nanocrystalline chemically homogeneous multilayers of type $[Fe_{100-x}\ Zr_x\ /^{57}\ Fe_{100-x}\ Zr_x]_{10}$, were performed using neutron reflectivity. On the basis of the results obtained, the self-diffusion mechanism in nanometer-range structures is discussed in this article.

1. Introduction

Amorphous and nanocrystalline metals and alloys, in which the tailoring of properties over a wide range by controlling particle size and morphology is possible, are an important class of materials.[1-4] Many physical properties, such as structural and magnetic properties, glass-to-crystal transition, and surface morphology, are strongly influenced by self-diffusion of the constituents. Further, the long-standing application of devices based on amorphous and nanocrystalline alloys is fundamentally controlled by the self-diffusion process. Therefore, an understanding of the self-diffusion mechanism is very important from both a scientific as well as technological point of view. To determine the self-diffusion mechanism, one needs to fabricate structures with proper isotopic labeling. Further, to probe structures with isotopic labeling, techniques capable of distinguishing contrast among isotopes are required. Mass spectrometry and radioactive tracer techniques have been used widely to probe self-diffusion.[5,6] These techniques essentially use cross sectioning and/or depth profiling to probe the buried layers. The depth resolution attained with these techniques is limited to about 5 nm, which poses a limit to the diffusion lengths that could be probed using these techniques. To probe self-diffusion lengths below this limit, a technique with much lower resolution is required.

It is known that the grazing incidence reflection of x-ray or neutron reflectometry (NR) is a nondestructive way to probe surfaces and even buried interfaces. The depth resolution available with reflectometry techniques is in the subnanometer-length scale (i.e., as low as 0.1 nm), and it makes them ideal for probing self-diffusion or interdiffusion in nanoscale structures. While x-rays are transparent for isotopes, neutrons do have significant contrast for many elements across the periodic table. This allows the use of neutrons for probing self-diffusion. Another technique that was proposed recently makes use of x-rays (synchrotron radiation [SR]) to probe self-diffusion in Mössbauer-active nuclei. This technique also is sensitive in the sub-nanometer-length scale but is limited to Mössbauer-active nuclei. This technique, which is called the nuclear resonant reflectivity of SR, uses nuclear resonance from the Mössbauer-active nuclei (e.g., ^{57}Fe).[7]

In the present work, NR has been used to investigate self-diffusion in amorphous and nanocrystalline samples of FeZr. Tailoring the composition of the alloy results in a variety of structures, and the aim of this work is to observe the influence of microstructure on self-diffusion process. This article is organized into four sections. Section 2 gives a brief introduction of the reflectometry technique with an emphasis on the methodology for determining self-diffusion. Section 3 explains the experimental part and gives details about the techniques used for sample preparation and measurement in this work. Section 4 presents the experimental results and describes the associated self-diffusion mechanism.

2. Neutron Reflectometry as a Probe to Investigate Self-Diffusion on the Nanometer Scale

Neutron reflectometry is a well-known technique for studying thin films and phenomena occurring at interfaces (for an overview, see Ref 8 and 9). The reflection of neutrons from a surface or an interface is similar to that of light or x-rays. However, there are three distinct differences with light or x-ray scattering: (a) weak absorption, in which neutrons interact with matter weakly and therefore have a deeper penetration depth compared with x-rays; (b) isotopic separation in which neutrons are scattered by nuclei while x-rays are scattered from electrons (an isotope of an element has different nuclei but the same number of electrons, which makes different scattering lengths for neutrons among isotopes of most of the elements); and (c) magnetic interaction,

This article is a revised version of the paper printed in the *Proceedings of the First International Conference on Diffusion in Solids and Liquids—DSL-2005*, Aveiro, Portugal, July 6-8, 2005, Andreas Öchsner, José Grácio and Frédéric Barlat, eds., University of Aveiro, 2005.

Mukul Gupta, Thomas Gutberlet, and **Rachana Gupta,** Laboratory for Neutron Scattering, ETH Zürich and Paul Scherrer Institute, CH-5232 Villigen PSI, Switzerland; and **Ajay Gupta,** UGC-DAE Consortium for Scientific Research, University Campus, Khandwa Road, Indore, IN-452017, India. Contact e-mail: mukul.gupta@psi.ch.

in which neutrons are chargeless spin 1/2 particles (due to the magnetic moment associated with their spin, they react equally to the presence of magnetic fields). The nuclear and magnetic interactions are similar in strength. For this reason, neutrons are an ideal probe for studying magnetic structure and dynamics.

Of the above-mentioned distinct advantages of neutron scattering, isotopic separation enables us to probe self-diffusion, provided that a proper isotopic labeling is incorporated. It is surprising to note that, despite substantial potential, NR has not been exploited sufficiently to investigate self-diffusion in metallic systems. Previous work carried out using NR is not extensive.[10-13] In principle, self-diffusivity can be obtained at an interface between two isotopic layers (e.g., ^{56}Fe/^{57}Fe). However, to enhance intensity, a multiple stack of such combinations is useful. When stacked in the form of a periodic multilayer (ML), Bragg peaks would appear corresponding to the period of the ML when measured using neutron reflectivity, whereas for x-rays no Bragg peak is expected due to the absence of contrast between the isotopes. As a matter of fact, x-ray reflectivity (XRR) measurements give direct proof that there is indeed no contrast between the isotopic layers, which is prerequisite to measure only self-diffusion.

Figure 1 shows an example of the FeZr/^{57}FeZr ML coated on an Si (100) substrate. As expected, the x-ray reflectivity (XRR) pattern (Fig. 1b) shows oscillations corresponding to the total thickness of the sample, while NR gives a Bragg peak (Fig. 1a) at the designed period, and a total thickness oscillation can also seen. The reflectivity of the ML can be calculated using the formalism of Parratt[14] by coherently summing the reflected amplitudes. It is known that reflectivity drops off as a function of q^4 for qq_c due to Fresnel reflectivity, where q is the momentum transfer vector given as $q = 4\pi\sin\theta/\lambda$ (where θ is the incident angle and λ is the wavelength of the radiation) and q_c is a critical value of q, where radiation starts penetrating into the sample, and below q_c incoming radiation is totally reflected off the surface.[14]

To calculate diffusivity, the intensity at the Bragg peak should be measured carefully, and this could be achieved by multiplying the reflectivity data by a factor of q^4. Such a multiplication results in a flat background due to the removal of q^4 dependence, making it easier to fit the data to a suitable function. To enhance diffusion, the ML has to be annealed at a sufficiently high temperature. As the ML is annealed, the intensity at the Bragg peak decreases. The diffusivity can be calculated without taking recourse to a detailed fitting of the reflectivity pattern, simply from the differences in the intensity before and after annealing. The equation for the calculation of diffusivity can be derived in the following way.

Taking the z direction perpendicular to the surface of the ML, the concentration of the modulating isotope (e.g., ^{57}Fe) can be defined as a periodic function of z by the Fourier series[15]:

$$C(z) = \sum_n C_n \exp(ik_n z), \qquad \text{(Eq 1)}$$

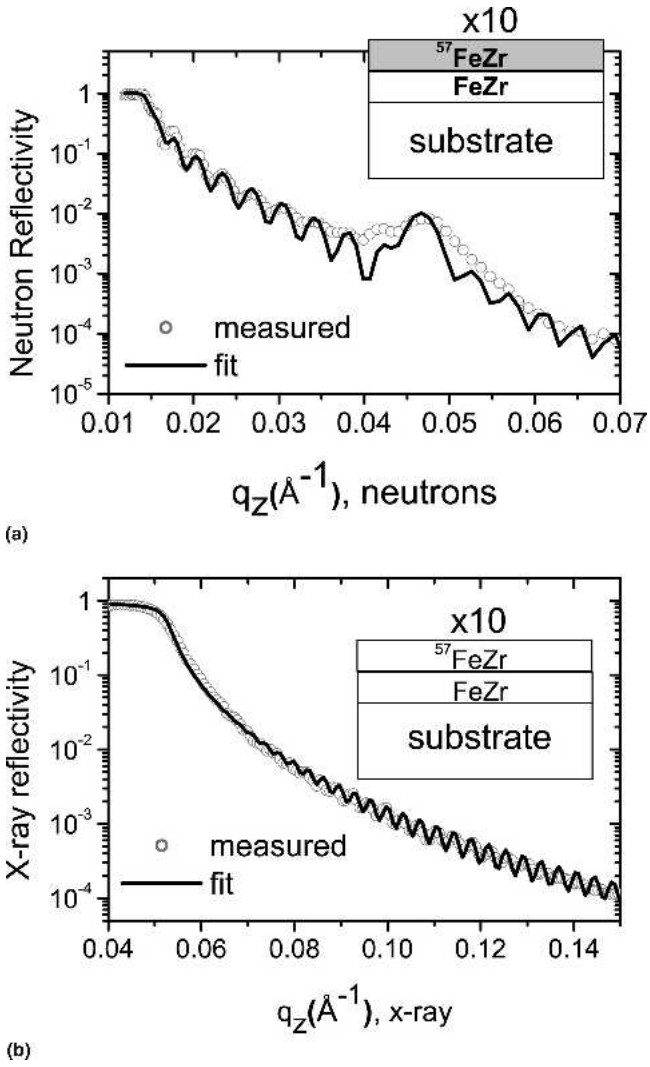

Fig. 1 (a) Neutron and (b) x-ray reflectivity of Si/[$Fe_{32}Zr_{68}$ (9.6 nm)/$^{57}Fe_{32}Zr_{64}$ (4.8 nm)]$_{10}$ ML

where $k_n = 2n\pi/d$ is the wave number of the nth harmonic, the period of which is d. After annealing due to interdiffusion, with amplitude decay C_n, annealing temperature T, and annealing time t, the one-dimensional diffusion equation can be written as:

$$C_n = C_{n0}\exp[-k_n^2 D(T)t], \qquad \text{(Eq 2)}$$

where $D(T)$ is the diffusivity at temperature T. The intensity at the nth Bragg peak is proportional to the square of amplitude C_n and can be written as:

$$\ln[I(t)/I(0)] = -8\pi^2 n^2 D(T)t/d^2, \qquad \text{(Eq 3)}$$

where $I(0)$ is the intensity before annealing and $I(t)$ is the intensity after t at T. The diffusion length L_d is related to diffusivity through the relation:

$$L_d = \sqrt{2D(T)t} \qquad \text{(Eq 4)}$$

Therefore, by monitoring the intensity at the Bragg peak

diffusivity and diffusion length can be obtained. Because atomic diffusion is a thermally activated process, it follows an Arrhenius-type relation given by:

$$D = D_0 \exp(-E/k_B T), \quad \text{(Eq 5)}$$

where E is the activation energy and D_0 is the preexponential factor.

Using Eq 3 to 5, self-diffusion, activation energy, and preexponential factor can be calculated for an ML by measuring NR as a function of annealing time and temperature. Due to a depth resolution as low as 0.1 nm, diffusion lengths as small as a fraction of a nanometer can be measured.

3. Experimental

3.1 Sample Preparation

The samples in this work have been prepared using direct current (dc)-magnetron sputtering operating at a power of 50 W at room temperature (with no intentional heating) on Si (100) or float glass substrates. Both Fe and Zr targets were cosputtered using an Fe + Zr composite target covering different ratios of Fe and Zr to obtain different compositions. The composition of the deposited alloy was measured using x-ray photoelectron spectroscopy. Pure Ar gas was used as a sputtering gas to deposit the alloy. The substrates were oscillated with respect to the center of the target to ensure better uniformity of the deposited samples. The substrates were placed at a distance of about 8 cm from the target. The pressure during the deposition was on the order of 4×10^{-3} mbar, while base pressure before the start of deposition was in the range of 1×10^{-6} mbar. The targets were presputtered for at least 10 min to remove contamination that might be absorbed at the surface when exposed to air. To prepare MLs with isotopic separation, natural Fe + Zr and ^{57}Fe + Zr targets were sputtered alternatively. The FeZr samples were also prepared as a function of applied stress. A stress was applied to understand the diffusion mechanism. The substrates were mounted on a specially designed 3-point Si wafer-bending device. The Si wafer was fixed from both the ends, and by the rotation of an asymmetric steel roller around the central axis the bending height of the Si wafer b can be varied between 0 and 5 mm. A pin-lock system was incorporated so that the release of bending by itself can be avoided. A compressive stress is applied to the deposited film when the bending of the Si wafer was released after deposition (the samples were deposited while Si wafer was bent). The stress that is applied to the Si wafer as a result of the release of bending can be calculated using the formula of Stoney[16] and following a discussion with Chen and De Wolfe.[17] The applied stress σ is given by:

$$\sigma = \frac{Y_{si} T^2}{6RT_f} \quad \text{(Eq 6)}$$

Where Y_{Si} is the biaxial modulus of the silicon substrate and is equal to: $Y_{Si} = E_{Si}/(1 - \nu_{Si})$, where E_{Si} is the Young's modulus for Si and ν_{Si} is Poisson's ratio for Si. The biaxial modulus of the silicon substrate is equal to 180.5 GPa. T_{Si} is the thickness of the substrate, T_f is the thickness of the film, and R is the radius of curvature. The R value can be calculated with the known bending length of the wafer a and the bending height b using the expression $R = a^2 + b^2/2b$, which could be followed from the geometry shown in Fig. 2.

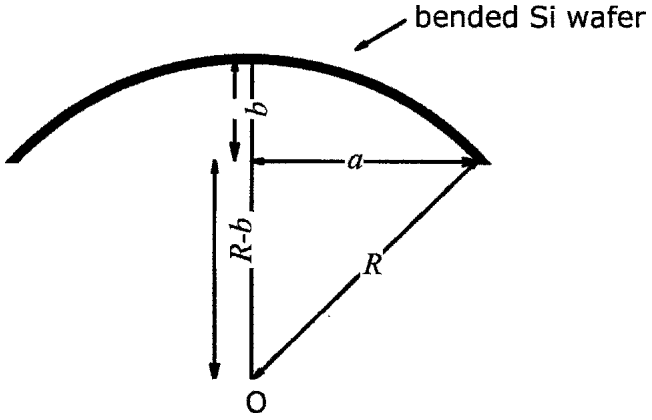

Fig. 2 Schematic diagram of the bent Si wafer used for the calculation of R

Using Eq 6, the value of stress can be calculated. The parameters used in the present case are $T_S = (300 \pm 10)$ μm, $T_f = 370$ nm, and $a = 40$ mm, and b was varied at 0, 3, and 5 mm. The obtained values of stress for the three cases are 0, 27, and 46 GPa. The errors in the calculation of applied stress were on the order of 15 to 20%, taking into account the uncertainties in the measured physical parameters. Samples with different known bending were deposited under similar deposition conditions. After deposition and the release of bending, the surface profile of the samples was measured using a profilometer. It was found that the surface of the samples was flat, and no changes in the surface profile were observed for a sample prepared with or without bending. This indicated that even after the bending the substrate gains its original state and the stress is applied on the deposited ML.

3.2 Measurement Techniques

Deposited samples were characterized for structural and magnetic properties using grazing incidence x-ray diffraction (GIXRD) and dc-extraction magnetometry with the physical properties measurement system. The thickness and roughness of the film was obtained using XRR. For measurements with x-rays, Cu-Kα radiation was used. Because the thickness of the films lies in the range of a few hundred nanometers, the GIXRD technique was used to reduce the background due to diffraction from the substrates. The incident angle was kept fixed just above the critical angle of the film in asymmetric Bragg-Brentano geometry, so that the penetration of the incident radiation is limited to the thickness of the film. Prior to diffusion measurements, the thermal stability of the deposited MLs was checked by an-

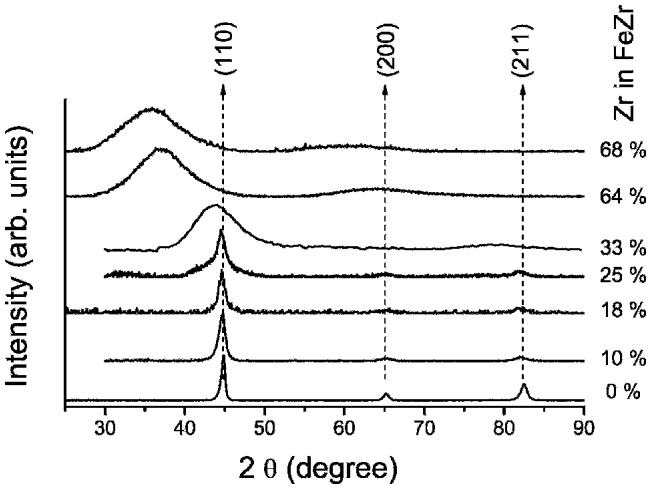

Fig. 3 The GIXRD pattern of FeZr thin films as a function of varying composition

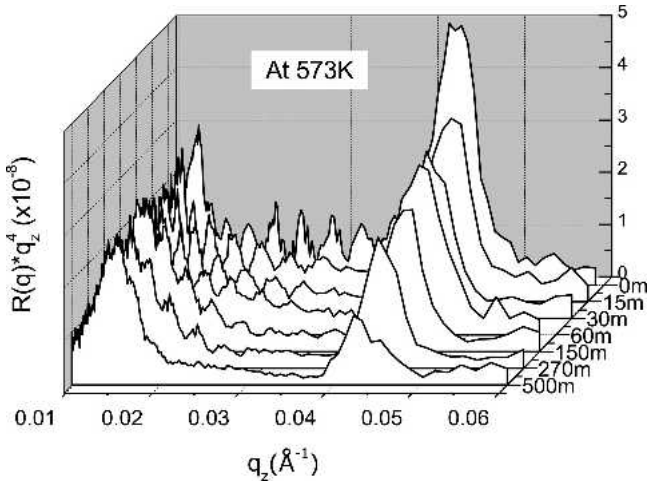

Fig. 4 The neutron reflectivity pattern of the Si/$[Fe_{36}Zr_{64}/{}^{57}Fe_{36}Zr_{64}]_{10}$ ML measured at 573 K as function of annealing time

nealing the samples in a vacuum furnace with a base pressure of about 1×10^{-6} mbar. The GIXRD and XRR measurements were carried out after each annealing to observe changes in the structure of the samples imposed due to thermal annealing. The crystallization behavior of the amorphous samples was examined using a NETZSCH (Germany, www.netzsch.com) differential scanning calorimeter equipped with an extremely high-sensitivity μ sensor. Such a sensor was required because of the very small mass of the samples. Diffusion measurements were carried out using neutron reflectometry (NR) known as AMOR at the Swiss Spallation neutron source (SINQ) in Paul Scherrer Institute (PSI), Switzerland in the time-of-flight (TOF) mode. The samples were heated using an in situ vacuum furnace that was specially designed to carry out NR measurements. The reason for using the TOF mode was the fact that in TOF mode the sample is fixed at an incident angle and the changes imposed by in situ thermal annealing can be measured without physically moving the sample or the detector.

4. Fe Self-Diffusion in Amorphous and Nanocrystalline FeZr

4.1 Composition Dependence

Fe self-diffusion in chemically homogeneous MLs of FeZr was measured as a function of composition and applied compressive stress during deposition. While compressive stress was applied for the sample with about 25% Zr, the composition dependence of Fe self-diffusion in FeZr was obtained for all of the samples (except for pure Fe), as shown in Fig. 3.

As can be seen from Fig. 3, as the amount of Zr (in atomic percent) is increased, the peak corresponding to (110) reflection of body-centered cubic (bcc) Fe starts becoming broadened. While it shifts to lower angles for Zr ≥ 64 at.%, high-temperature annealing of samples above 64 at.% Zr predominantly produces a Zr-rich Zr_3Fe phase, indicating that the amorphous phase produced for Zr-rich samples corresponds to an intermetallic alloy, Zr_3Fe. The Fe-rich phases are solid solutions of Fe and Zr with a bcc structure. The crystallization temperature of the amorphous alloy increases as the Zr content is increased. The annealing of the samples with Zr < 25 at.% at 373 K resulted in a mixture of amorphous and nanocrystalline phases. The Fe self-diffusion measurements for samples with Zr < 25 at.% were carried out in the metastable nanocomposite phase, while for the samples with Zr > 25 at.% they were carried out in the amorphous phase.

As an example, the results of self-diffusion measurements in amorphous $Fe_{36}Zr_{64}$ are demonstrated here. Figure 4 shows the neutron reflectivity pattern of the MLs before and after annealing at 573 K for different amounts of time. As the time of annealing is increased, the intensity at the Bragg peak gradually decreases. Following Eq 3 and 4, diffusivity and diffusion length can be obtained.

Figure 5 shows a plot of the square of the diffusion length as a function of annealing time at different temperatures. It can bee seen from Fig. 5 that at all annealing temperatures the diffusion length initially increases at a faster rate and that after a certain annealing time the rate becomes constant. The initial faster increase in the diffusion length may be associated with the structural relaxation in the system. Earlier studies have shown that amorphous alloys exhibit structural relaxation, which is associated with annihilation of the free volume due to thermal annealing. Because during relaxation the diffusivity is higher, the initial points are excluded form the fitted line. As expected, relaxation is faster at higher temperatures. In the well-relaxed state, ln D and $1/T$ follow the Arrhenius-type behavior given in Eq 5, yielding the preexponential factor and activation energy shown in Fig. 6. Similarly, self-diffusion measurements have been performed for samples having different amounts of Zr and in FeZr. While comparable to the activation energy for bulk diffusion in $Fe_{91}Zr_9$,[18,19] the value of activation energy in the present case is significantly smaller in all compositions (Fig. 7). It may be noted that the activation energy for Fe self-diffusion remains almost constant in the nanocomposite samples, whereas it increases marginally in

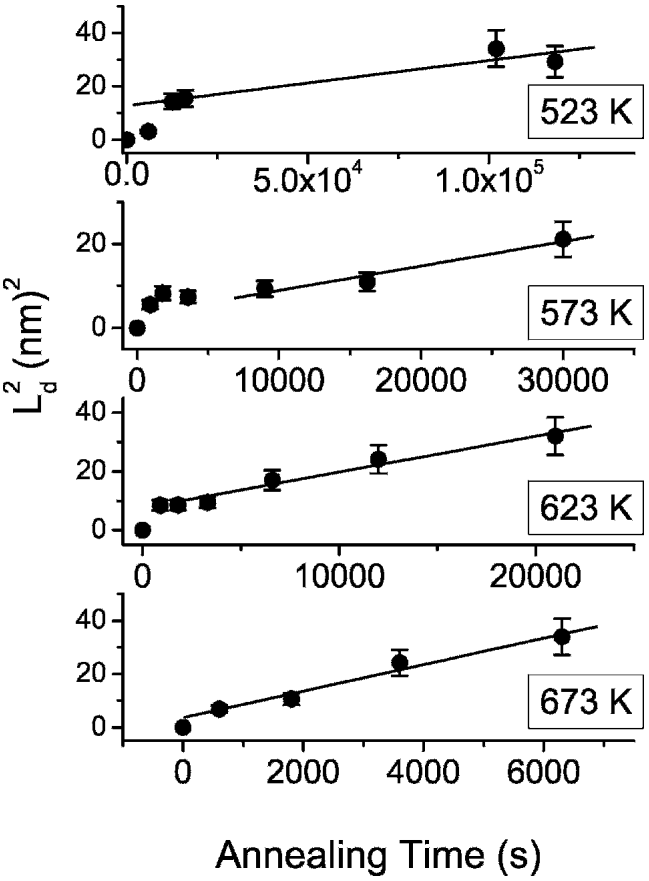

Fig. 5 The evolution of the square of the diffusion length as a function of annealing time. Straight-line fits have been obtained using Eq 4.

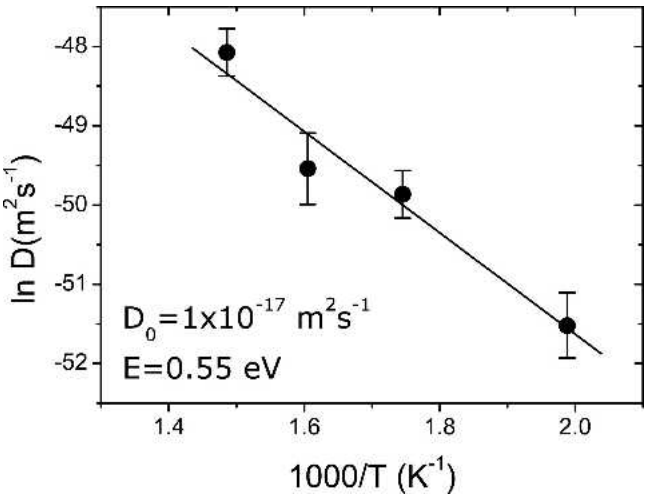

Fig. 6 Arrhenius behavior of diffusivity. Straight-line fits have been obtained using Eq 5.

the amorphous phase (Zr = 33 at.%). Further, close to the equiatomic composition there is a marked increase in the activation energy, as shown in Fig. 7.

In the case of three-dimensional transition metal/Zr bi-

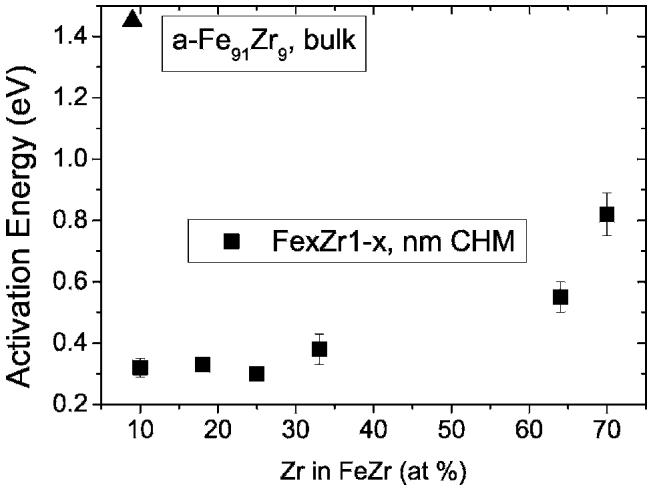

Fig. 7 Variation in activation energy for the self-diffusion of Fe as a function of Zr in FeZr

nary alloys, at low Zr concentrations the structure is relatively loosely packed with Zr atoms filling the low-density region. As the Zr content is increased, the structure becomes more rigid. At equiatomic concentrations, a more densely packed structure with a rigid Zr backbone is obtained, as observed in CoZr.[6] Therefore, it is expected that diffusivity would change with increasing Zr content. An increase in activation energy is directly related to a decrease in diffusivity. As pointed out by Rössler and Teichler,[20] in their molecular dynamics simulation of an amorphous CoZr alloy in which the Zr atoms are dragged along with the flow of the Co atoms with low Zr contents, while at higher Zr contents the dense Zr substructure impedes Co movements. The nature of Fe diffusion in the present case can be understood in the same way.

4.2 Effect of Applied Compressive Stress

It is known that the pressure/stress dependence of diffusivity is the key for the determination of the associated diffusion mechanism.[21] For a case in which diffusion takes place via defects in thermal equilibrium, one expects an activation volume on the order of the size of a defect (i.e., one atomic volume for a single jump vacancy diffusion). For a diffusion process without thermally generated defects, the activation volume should nearly vanish.[22] To get further insight into the diffusion mechanism, structures with different applied stresses were prepared, as discussed in the previous section. Chemically homogeneous MLs with structures Si (substrate)/[$Fe_{75}Zr_{25}$ (25 nm)/$^{57}Fe_{75}Zr_{25}$ (10 nm)]$_{10}$ were deposited onto Si (100) substrates, which are bent to different curvatures, as described in section 3. A release of bending causes a uniaxial compressive stress in the deposited ML. The self-diffusion of Fe in these MLs has been studied by annealing all of the MLs together in the temperature range of 373 to 533 K, where a nanocomposite structure is formed. The decay of the intensity at the Bragg peak positions was measured as a function of annealing time and temperature. Figure 8 shows the evolution of diffusion

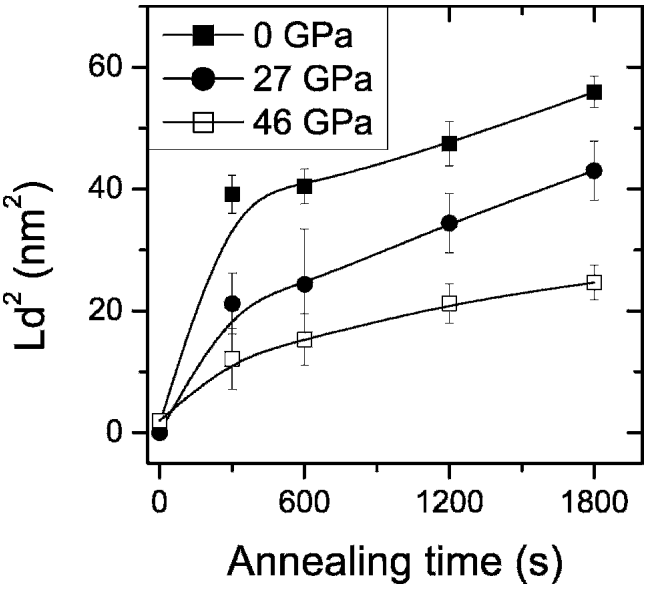

Fig. 8 The evolution of diffusion length as a function of annealing time and applied stress at 473 K. The solid lines are a guide for the eye.

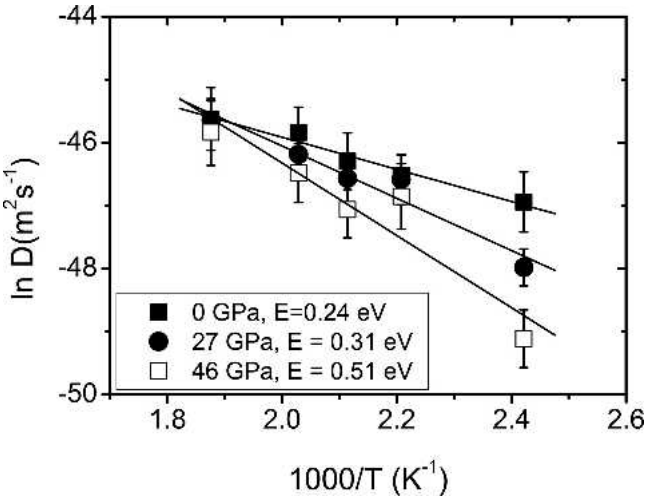

Fig. 9 Arrhenius behavior of the diffusivity of samples with applied stresses of 0, 27, and 46 GPa

length at 473 K for the samples prepared using applied stresses of 0, 27, and 46 GPa. It is interesting to see that for the sample prepared without any stress, the diffusion length increased much faster compared with the samples prepared with an applied stress, indicating that samples prepared with an applied stress exhibited a more relaxed state compared with that obtained without an applied stress. It is expected that structural relaxation would be more dominant for the sample prepared without an applied stress. The overall magnitude of the diffusion length follows the strength of applied stress, and the degree of relaxation is proportional.

Similarly, measurements were performed at different temperatures, and Fig. 9 shows a plot of diffusivities for the sample at 0, 27, and 46 GPa. The activation energy was found to increase with an increase in the strength of applied compressive stress (a steeper slope was observed with an increase in the applied stress). This result gives a clear indication that diffusivity for the sample prepared with applied stress is much slower compared with that prepared without applied stress. The diffusivity at 413 K shows the largest variation with applied stress, while at the highest temperature (533 K) the diffusivity for all of the applied stress was found to be almost similar. Because in the present case the stress was applied only in the uniaxial direction, the activation volume available for diffusion could not be calculated; therefore, direct correlations with the values reported in the literature could not be made as the pressure applied in those studies was hydrostatic in nature. However, in the present case, even though the stress is applied in the uniaxial direction, the effect of applied stress is significant. An increase in activation energy with an applied stress clearly indicates the more relaxed state of the alloy when stress is applied due to the release of bending. Further, at 533 K the fact that the effect of applied stress vanishes and the diffusivity in all the cases is similar indicates a compensation-type effect that is induced by thermal annealing. The samples prepared without applied stress are in a highly stressed state brought on mainly by the deposition process.

An applied stress results in the partial release of these stresses, which further relaxes at higher temperatures. At a sufficiently high temperature, the alloy attains a fully relaxed state and diffusivities at this point converge. The values of activation energies, E, and the preexponential factor D_0 for Fe self-diffusion that was obtained in the present case can be compared with those reported in the literature for amorphous alloys. It is well known that a correlation between E (or H) and D_0 exists for self-diffusion and impurity diffusion in conventional and bulk amorphous alloys, and even for nanocrystalline and crystalline alloys. This relationship seems to have a universal character because it has been observed not only for self-diffusion and impurity diffusion in amorphous alloys but also in nanocrystalline and crystalline alloys, as shown in Fig. 10.[6] The relationship between E and D_0 is known as the *isokinetic relation* and is given by[23]:

$$\ln D_0 = \ln \mathrm{A} + E/\mathrm{B} \qquad \text{(Eq 7)}$$

where A and B are constants. Taking the data point obtained in the present case (Fig. 10), the values of A and B are approximately 2×10^{-20} and 0.056, respectively, which are close to the values obtained for diffusion in amorphous alloys and for interdiffusion in chemically inhomogeneous metallic MLs. Following the approach discussed by Shewmon,[24] the preexponential factor D_0 can be expressed as:

$$\ln D_0 = \ln(ga^2 f\nu_0) + \Delta S/k_\mathrm{B} \qquad \text{(Eq 8)}$$

where g is a geometry factor, a is the effective jump distance, ν_0 is the effective jump attempt frequency, f is a correlation factor, and ΔS is the entropy for diffusion. Using Eq 7 and 8, the values for the constants A and B can be written as:

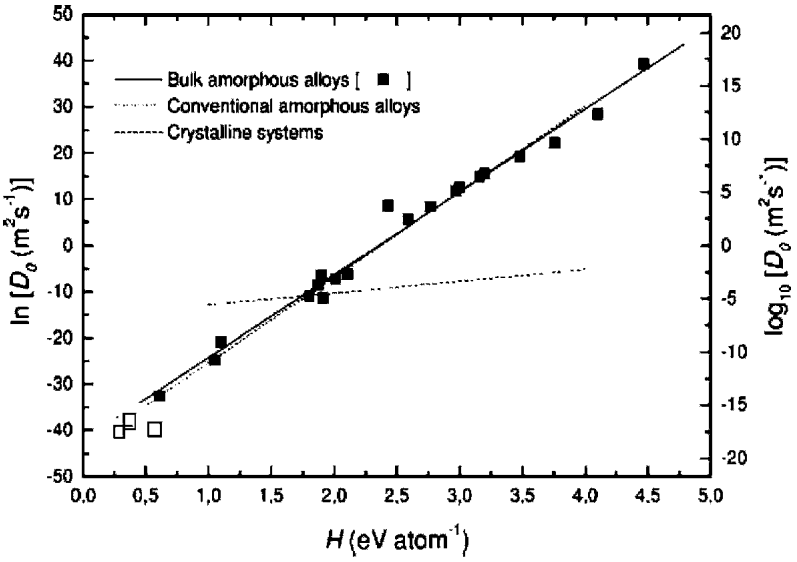

Fig. 10 The E (or H)-D_0 correlation for diffusion in various alloys.[6] The open square symbol (□), corresponds to the present study.

$$A = ga^2 f\nu_0,\ B = k_B E/\Delta S \quad \text{(Eq 9)}$$

With the obtained values of B and E, the entropy term for the present sample would be in the range of 5 to 10 k_B (Boltzmann constant) (in order of increasing Zr atomic percent), which is significantly smaller compared with the range of 20 to 50 k_B observed for bulk amorphous alloys. The value of ΔS in the range of 5 to 10 k_B would roughly correspond to a group of atoms consisting of 5 to 10 atoms that participate in the diffusion mechanism. Contrary to the case in bulk amorphous alloys, where a cluster of 20 to 60 atoms participate in the diffusion mechanism, making it highly collective in nature, in chemically homogeneous MLs a smaller number of atoms participate. This means that diffusion in the chemically homogenous ML is not highly collective but would involve a relatively small group of atoms, indicating a much faster diffusion compared with that of bulk amorphous alloys.

5. Conclusions

It can be seen from the current study that neutron reflectivity is a unique technique with which to probe self-diffusion in a nanoscale structure with depth resolution in a subnanometer range. Using proper isotopic labeling, neutron reflectivity can be used in a number of systems to probe self-diffusion. The results obtained from the current study show that the Fe self-diffusion mechanism in amorphous FeZr MLs is not highly collective as observed in the case of bulk alloy, but involves a rather small group of atoms. The effect of applied compressive stress results in the partial relaxation of the FeZr alloy, making the diffusive motion slower.

Acknowledgments

The authors would like to thank M. Horisberger for providing help with thin film deposition and H. Grimmer for access to an x-ray machine. This work was performed at the Swiss Spallation Neutron Source, Paul Scherrer Institute, Villigen, Switzerland.

References

1. P.G. Debenedetti and F.H. Stillinger, Supercooled Liquids and the Glass Transition, *Nature,* Vol 410, 2001, p 259-267
2. C.A. Angell, K.L. Nagi, G.B. McKenna, P.F. McMillan, and S.W.J. Martin, Relaxation in Glassforming Liquids and Amorphous Solids, *J. Appl. Phys.,* Vol 88, 2000, p 3113
3. A. Dunlop, G. Jaskierowicz, G. Rizza, and M. Kopcewicz, Partial Crystallization of an Amorphous Alloy by Electronic Energy Deposition, *Phys. Rev. Lett.,* Vol 90, 2003, p 015503
4. M.E. McHenry, M.A. Willard, and D.E. Laughlin, Amorphous and Nanocrystalline Materials for Applications as Soft Magnets, *Prog. Mater. Sci.,* Vol 44, 1999, p 291-433
5. M. Gupta, A. Gupta, S. Rajagopalan, and A.K. Tyagi, Self-Diffusion of Iron in Amorphous Iron Nitride, *Phys. Rev. B: Condens. Matter,* Vol 65, 2002, p 214204
6. F. Faupel, W. Frank, M.P. Macht, H. Mehrer, K. Rätzke, H.R. Schober, S.K. Sharma, and H. Teichler, Diffusion in Metallic Glasses and Supercooled Melts, *Rev. Mod. Phys.,* Vol 75, 2003, p 237
7. A. Gupta, M. Gupta, S. Chakravarty, R. R̈uffer, H.-C. Wille, and O. Leupold, Fe Diffusion in Amorphous and Nanocrystalline Alloys Studied Using Nuclear Resonance Reflectivity, *Phys. Rev. B: Condens. Matter,* Vol 72, 2005, p 014207
8. J. Penfold and R.K. Thomas, The Application of the Specular Reflection of Neutrons to the Study of Surfaces and Interfaces, *J. Phys.: Condens. Matter,* Vol 2, 1990, p 1369
9. S.K. Sinha, E.B. Sirota, S. Garoff, and H.B. Stanley, X-ray and Neutron Scattering from Rough Surfaces, *Phys. Rev. B: Condens. Matter,* Vol 38, 1988, p 2297
10. A.L. Greer, Diffusion and Phase Nucleation in Metallic Multilayers, *J. Magn. Magn., Mater.,* Vol 126, 1993, p 89
11. J. Speakman, P. Rose, J.A. Hunt, N. Cowlam, R.E. Somekh, and A.L. Greer, *J. Magn. Magn., Mater.,* Vol 156, 1996, p 411
12. S.M. Baker, G.S. Smith, N.J.S. Brown, M. Nastasi, and K. Hubbard, Observation of Nonstandard Fickian Diffusion at the Interface of Isotopically Pure Amorphous 11B on 10B by

Neutron Reflectometry, *Phys. Rev. B: Condens. Matter,* Vol 55, 1997, p 7255
13. M. Gupta, A. Gupta, J. Stahn, M. Horisberger, T. Gutberlet, and P. Allenspach, Iron Self-Diffusion in Amorphous FeZr/57FeZr Multilayers Measured by Neutron Reflectometry, *Phys. Rev. B: Condens. Matter,* Vol 70, 2004, 184206
14. L.G. Parratt, Surface Studies of Solids by Total Reflection of X-Rays, *Phys. Rev. B: Condens. Matter,* Vol 95, 1954, p 359
15. T. Mizoguchi and M. Murata, Free-Volume-Dependent Atomic Diffusion in Compositionally Modulated Amorphous Co-Zr Films, *Jpn. J. Appl. Phys.,* Vol 30, 1991, p 1818
16. G.G. Stoney, *Proc. R. Soc. A,* London, Ser. Vol 82, 1909, p 172
17. J. Chen and I. De Wolf, Study of Damage and Stress Induced by Backgrinding in Si Wafers, *Semicond. Sci. Technol.,* Vol 18, 2003, p 261
18. J. Horvath, J. Ott, K. Pfahler, and W. Ulfert, Tracer Diffusion in Amorphous Alloys, *Mater. Sci. Eng.,* Vol 97, 1988, p 409
19. H. Kronmüller and W. Frank, Unified Analysis of Diffusion and Relaxation Processes in Amorphous Metallic Alloys, *Radiat. Eff. Defects Solids,* Vol 108, 1989, p 81
20. U.K. Rössler and H. Teichler, Molecular Dynamics Simulations of Supercooled and Amorphous Co100-xZrx: Atomic Mobilities and Structural Properties, *Phys. Rev. E, Stat. Phys., Plasmas, Fluids, Relat. Interdiscip. Top.,* Vol 61, 2000, p 394
21. P. Klugkist, K. Rätzke, S. Rehders, P. Troche, and F. Faupel, Activation Volume of 57Co Diffusion in Amorphous Co81Zr19, *Phys. Rev. Lett.,* Vol 80, 1998, p 3288
22. H. Mehrer, Ed., *Diffusion in Solid Metals and Alloys,* Vol. 26, Landolt-Börnstein, New Series, Group III, Springer-Verlag, Berlin, 1991
23. W. Linert, The Isokinetic Relationship, *Chem. Soc. Rev.,* Vol 18, 1989, p 477
24. P.G. Shewmon, *Diffusion in Solids, Minerals, Metals, and Materials Society,* Warrendale, PA, 1989